

Probing interstellar extinction near the 30 Doradus nebula with red giant stars^{*}

Guido De Marchi,¹ Nino Panagia,^{2,3,4} and Léo Girardi⁵

¹European Space Research and Technology Centre, Keplerlaan 1, 2200 AG Noordwijk, The Netherlands, gdemarchi@rssd.esa.int

²Space Telescope Science Institute, 3700 San Martin Drive, Baltimore, MD 21218, USA, panagia@stsci.edu

³INAF–NA, Osservatorio Astronomico di Capodimonte, Salita Moiariello 16, 80131 Naples, Italy

⁴Supernova Ltd, OYV #131, Northsound Rd., Virgin Gorda VG1150, Virgin Islands, UK

⁵INAF–PD, Osservatorio Astronomico di Padova, Vicolo Osservatorio 5, 35122 Padua, Italy, leo.girardi@oapd.inaf.it

Received 9.10.2013; Accepted 13.11.2013

ABSTRACT

We have studied the interstellar extinction in a field of $\sim 3' \times 3'$ located about $6'$ SW of 30 Doradus in the Large Magellanic Cloud (LMC). *Hubble Space Telescope* observations in the U , B , V , I and $H\alpha$ bands reveal patchy extinction in this field. The colour–magnitude diagram (CMD) shows an elongated stellar sequence, almost parallel to the main sequence (MS), which is in reality made up of stars of the red giant clump (RC) spread across the CMD by the uneven levels of extinction in this region. Since these objects are all at the same distance from us and share very similar physical properties, we can derive quantitatively both the extinction law in the range $3\,000 - 8\,000 \text{ \AA}$ and the absolute extinction towards about 100 objects, setting statistically significant constraints on the dust grains properties in this area. We find an extinction curve considerably flatter than the standard Galactic one and than those obtained before for the LMC. The derived value of $R_V = 5.6 \pm 0.3$ implies that in this region larger grains dominate. Upper MS stars span a narrower range of $E(B - V)$ values than RC objects, at variance with what has been found elsewhere in the LMC.

Key words: Hertzsprung–Russell and colour–magnitude diagrams — dust, extinction — Magellanic Clouds

1 INTRODUCTION

The traditional approach to deriving extinction curves is the “pair method,” in which the flux distribution or colours of a reddened object are compared with those of a star of the same spectral type (e.g. Massa, Savage & Fitzpatrick 1983; Cardelli et al. 1992; and references therein). This is possible because the interstellar extinction A_λ towards a given star can be determined by the ratio of its observed spectral energy distribution $F_{\text{obs}}(\lambda)$ and the expected or intrinsic spectrum for this star $F_{\text{exp}}(\lambda)$, i.e.

$$A_\lambda = -2.5 \times \log \frac{F_{\text{obs}}(\lambda)}{F_{\text{exp}}(\lambda)} \quad (1)$$

In principle, the expected spectrum should be the one appropriate for an extinction-free star with the same spectral type, the same absolute luminosity and the same distance as the target star. Since in general it is very hard to satisfy these conditions accurately, most of the studies are done considering the colour excess, $E_\lambda(\lambda, \lambda_0)$, defined as

$$E_\lambda(\lambda, \lambda_0) = A_\lambda - A_{\lambda_0} = -2.5 \times \log \left[\frac{F_\lambda / F_{\lambda_0}}{F_{\lambda, \text{ref}} / F_{\lambda_0, \text{ref}}} \right] \quad (2)$$

Dealing with a ratio of ratios, this quantity is independent of the distance to the stars considered as well as of their radii. Moreover, to separate the behaviour of the extinction from its absolute value for different pairs of stars or, equivalently, for different lines of sight, the colour excess is usually normalized. It is customary to take the ratio between a colour excess and the one in a reference wavelength interval (λ_1, λ_0) , i.e.

$$\mathcal{E}(\lambda, \lambda_0) = \frac{E(\lambda, \lambda_0)}{E(\lambda_1, \lambda_0)}, \quad (3)$$

which for example for $\lambda_1 = \lambda_B \simeq 4350 \text{ \AA}$, and $\lambda_0 = \lambda_V \simeq 5500 \text{ \AA}$ becomes $E(\lambda - V)/E(B - V)$. The colour excess normalized in this way is the form usually adopted to describe the extinction curve, i.e. the run of the selective extinction, suitably normalized, as a function of the wavelength λ .

We note that an implicit assumption underlying this procedure is that the extinction law is the same for all pairs of stars. With this procedure we can study and compare the slopes of the extinction laws between different stars and directions, and therefore derive relative dust properties, but still we do not have a charac-

^{*} Based on observations with the NASA/ESA *Hubble Space Telescope*, obtained at the Space Telescope Science Institute, which is operated by AURA, Inc., under NASA contract NAS5-26555.

terization of the absolute value of the extinction. The latter is usually expressed in terms of the absolute extinction A_λ/A_V at wavelength λ , comparing the total extinction at that wavelength with that in the V band. Alternatively, it is also given by the parameter $R_V \equiv A_V/E(B-V)$, which provides total to selective extinction in the B and V bands.

To derive the absolute extinction measurements have to be extended to very long wavelengths, taking advantage of the physical properties of dust grains, whose extinction cross-section tends to zero when the wavelength approaches infinity, i.e. $\lim_{\lambda \rightarrow \infty} A_\lambda = 0$, and therefore the colour excess $\mathcal{E}(\lambda, \lambda_0)$ becomes

$$\mathcal{E}(\lambda, \infty) = \frac{A_\lambda - A_\infty}{A_B - A_V} = \frac{A_\lambda}{E(B-V)}. \quad (4)$$

For many lines of sight accurate measurements today extend to the near-infrared, usually to the K band, and it is a common practice to estimate values for R_V from the extrapolation

$$R_V = \frac{E(V - \lambda_\infty)}{E(B - V)} \simeq 1.1 \frac{E(V - K)}{E(B - V)} \quad (5)$$

based on the assumption that the theoretical extinction curve no. 15 of van de Hulst (van de Hulst 1949, as reported by Johnson 1968) is appropriate for the interstellar medium under study. However, as Fitzpatrick & Massa (2007) already pointed out, this extrapolation is necessarily only accurate if $R_V \simeq 3$, since this is the value to which the van de Hulst's theoretical curve no. 15 applies, but it systematically deviates at higher and lower values of R_V .

That R_V varies considerably in our Galaxy is well known, particularly thanks to the studies conducted in the 1970's with the *Orbiting Astronomical Observatory 2* (Bless & Savage 1972), with the *Copernicus* and *TD-1* satellites (e.g. Seaton 1979), and later with the *International Ultraviolet Explorer*, which revealed a wide variety of extinction curves (see e.g. Fitzpatrick 1998, 1999 and references therein). Large variations are seen in the ultraviolet (UV) portion of the spectrum, with a more or less steep raise of the curve in the far-UV and a more or less prominent ‘‘bump’’ at 2 175 Å, and in smaller amount also at optical wavelengths.

Using the extrapolation to infinity mentioned above to derive R_V , Gordon et al. (2003) have carried out a quantitative comparison of all known extinction curves in the Large and Small Magellanic Clouds (LMC and SMC, respectively) with the Galactic curves. They find average R_V values of 2.05 ± 0.17 for the SMC wing (one star), 2.74 ± 0.13 for the SMC bar (four stars), 2.76 ± 0.09 for the LMC supershell near the 30 Dor region (eight stars) and 3.41 ± 0.06 for lines of sight to ten stars elsewhere in the LMC. Although these R_V values are not too different from the average value found in the diffuse Galactic interstellar medium ($R_V = 3.1$; e.g. Savage & Mathis 1979), the majority of the Magellanic Clouds (MC) extinction curves that Gordon et al. (2003) find are significantly different in the UV from the Milky Way (MW) extinction curves. These authors conclude that the environments probed by their observations, being biased towards active star forming regions, are rather different from those included in the sample studied by Cardelli et al. (1988, 1989), which is based on fairly quiescent lines of sight.

Recently, Haschke, Grebel & Duffau (2011), arguing that the differences between the MC extinction curves of Gordon et al. (2003) and the Galactic law by Cardelli et al. (1989) are quite small at optical wavelengths, concluded that the Cardelli et al. (1989) curve is generally a valid assumption also for the MC in that wavelength range. In fact, the differences appear small because the absolute extinction A_λ/A_V given by Gordon et al. (2003) is normalized

in the V band, but considerable differences between the MC and the Galaxy remain also at these wavelengths.

In this work we present a new method to unambiguously determine the absolute value of the extinction in the MC in all observed bands, deriving in this way an absolute extinction law. Our method, originally presented by Panagia & De Marchi (2005), makes use of multi-band photometry of red giant stars belonging to the red clump (RC).

Other authors have used RC observations before to study the reddening distribution and to derive reddening maps in the MC (e.g. Zaritsky 1999; Haschke et al. 2011; Tatton et al. 2013), for an assumed extinction curve. However, these observations do not provide an independent determination of the extinction curve in the MC. Recently, Nataf et al. (2013) used observations of RC stars in the Galactic bulge, collected as part of the Optical Gravitational Lensing Experiment (OGLE) project (Paczynski 1986), to determine the reddening and extinction towards the inner MW, finding a rather steep extinction curve ($R_V \simeq 2.5$). However, since only observations in the V and I bands are available as part of the OGLE project (supplemented by $E(J - K_s)$ measurements from other surveys), these results cannot be extended to shorter wavelengths.

Instead, the novelty and advantage of our method consists in the facts that (i) all stars on which we operate are at the same distance, to better than 1 %, (ii) they have very similar intrinsic physical properties in all bands, within 0.05 mag for similar age and metallicity, (iii) our statistics is very solid, with of the order of ~ 100 objects per field, and (iv) we derive a self-consistent *absolute* extinction curve over the entire optical range (3 000 – 8 000 Å) from photometry alone, without uncertain extrapolations from infrared bands. Our method, whose application is shown here for a field in the vicinity of the 30 Dor nebula in the LMC, can easily be extended to other nearby galaxies.

The structure of this paper is as follows. The observations and their analysis are presented in Section 2, while the results of the photometric reductions are shown in Section 3. The physical properties of the red giant clump are discussed in Section 4, while in Section 5 we proceed to deriving the absolute extinction law in the field of our study. Section 6 is devoted to a discussion of the reddening distribution in this field. A summary and our conclusions follow in Section 7.

2 OBSERVATIONS AND DATA ANALYSIS

The data used in our investigation were collected as part of the *Hubble Space Telescope (HST) / Wide Field Planetary Camera 2 (WFPC 2)* pure parallel programme (see Wadadekar et al. 2006) and cover a region of $\sim 2'.7$ on a side located at $\alpha = 5^{\text{h}}37^{\text{m}}49^{\text{s}}$, $\delta = -69^\circ 8' 18''$ (J2000), or about $6'$ SW of 30 Dor (NGC 2070). This region was observed with the WFPC 2 instrument (Mc Master & Biretta 2008) on board the HST on 2001 Jan 6 and 7 in several bands. Table 1 lists the total duration of the long exposures in each band. In addition to these, a series of short exposures (typically ~ 10 s duration) was collected in all bands to properly measure the magnitude of bright stars that would otherwise saturate.

A suitable dithering pattern was applied during the observations in order to make it possible to efficiently remove cosmic rays by comparing images taken through the same filter at different times.

The data were subjected to the automated standard reduction and pipeline procedure offered by the HST archive (‘‘on the fly calibration’’; Micol et al. 2000), which also took care of properly registering and co-adding images taken in the same band. The accu-

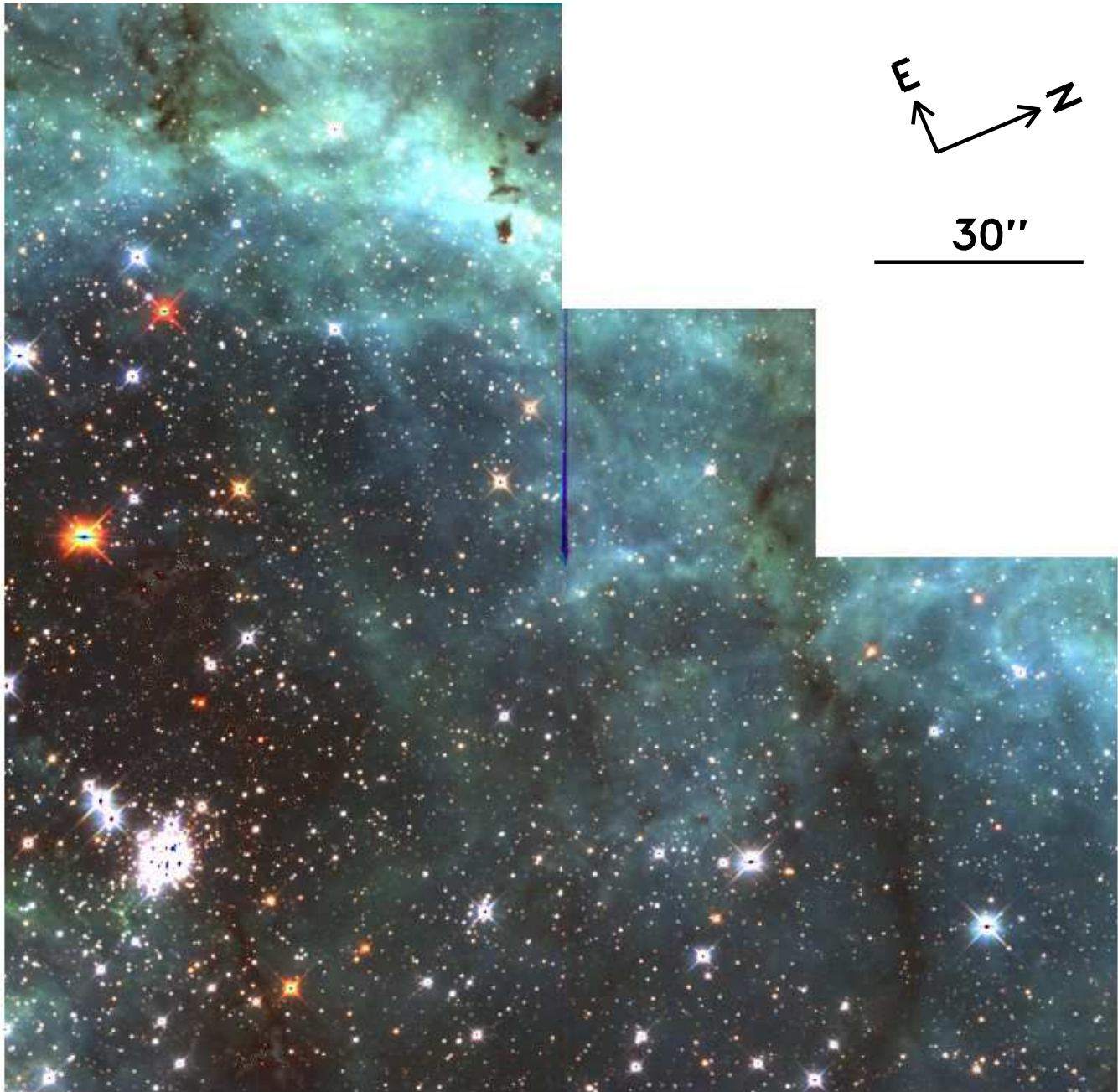


Figure 1. True colour image of a field of $2'.7 \times 2'.7$, located at RA= $5^{\text{h}}37^{\text{m}}49^{\text{s}}$, Dec= $-69^{\circ}8'18''$ (J 2000), or about $6'$ SW of 30 Dor. North is inclined $\sim 67^{\circ}$ clockwise with respect to the vertical, and east is to the left of north. In this figure, the exposure in the F300W band is used for the blue channel, the F450W image for the green channel, and the average of the F606W and F814W exposures for the red channel. In this work we only consider objects contained in the chips WF 2 (upper left), WF 3 (lower left) and WF 4 (lower right), whereas stars in the PC 1 chip (upper right) are not considered.

racy of the registration and combination procedures was verified by comparing the properties of the point spread function (PSF) in the individual images and in the combined ones. We find that the full width at half-maximum (FWHM) of stars in the combined frame increases by about 15 %, as is typical of any shift-and-add operation conducted on under-sampled images.

In Figure 1 we show a true-colour image obtained by combining the F450W, F606W and F814W frames with the F656N ($H\alpha$) observations. The $H\alpha$ image traces the extended nebulosity, which appears highly variable on scales of the order of $1''$ or ~ 0.25 pc at

the distance of the LMC (51.4 ± 1.2 kpc; Panagia et al. 1991, and updates in Panagia 1998, 1999). Several obscured regions are also present. It is, therefore, to be expected that the extinction will vary considerably across this field.

Object identification was carried out on the F814W combined frame, the deepest of the set, using the standard IRAF *ap-phot.daofind* routine. To guarantee that most noise spikes and PSF artefacts are automatically rejected, we conservatively set the detection threshold at 10σ above the local average background level. The automated procedure turned out about 8 830 stars in the three

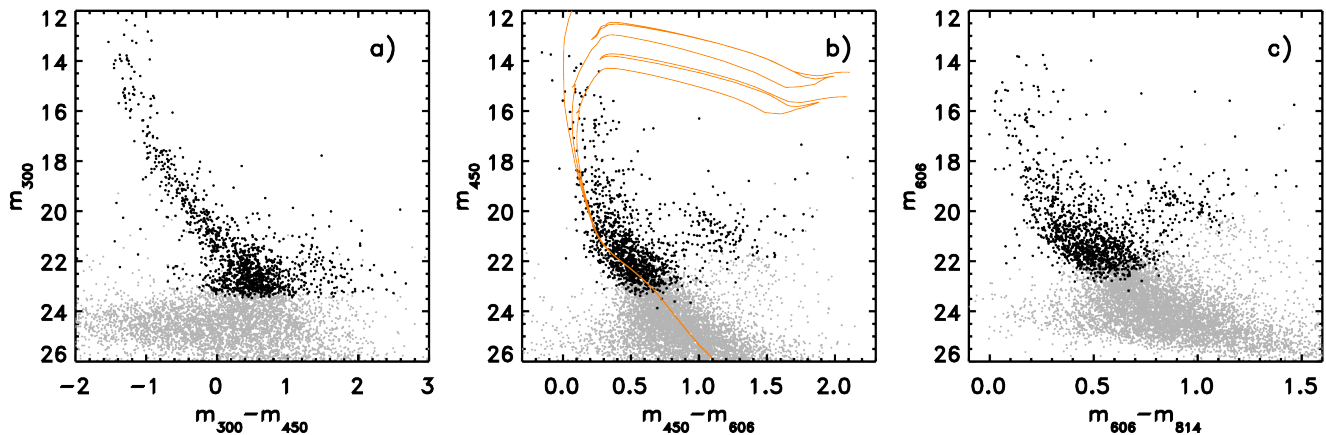


Figure 2. Colour–magnitude diagrams in the most common colour combinations. Thicker dots correspond to stars with $\delta_4 < 0.1$. The isochrones shown in panel b) correspond, from left to right, to ages of 4, 20 and 40 Myr for metallicity $Z = 0.008$.

Table 1. Cumulative exposure times in the various bands

Filter	Total exposure time
F300W (<i>U</i>)	2 800 s
F450W (<i>B</i>)	2 500 s
F606W (<i>V</i>)	2 900 s
F656N (<i>Hα</i>)	3 800 s
F814W (<i>I</i>)	3 200 s

wide field (WF) chips (we did not use the PC frame), all of which were carefully inspected by eye to remove saturated stars, a number of features above 10σ (PSF tendrils, noise spikes, etc.) that *daofind* had interpreted as stars, as well as a very few extended objects (with FWHM larger than twice that typical of point sources). The final object list pruned in this way includes about 8 350 well defined stars in the F814W band and was used as a master list for photometry in all frames in all bands.

Crowding not being severe, stellar fluxes were measured by using the standard IRAF *digiphot.apphot* aperture photometry routine, following the prescription of the “core aperture photometry” technique described in Gilmozzi & Panagia (1991) and De Marchi et al. (1993). In particular, we adopted an aperture radius of 2 pixel and a background annulus extending from 3 to 5 pixel in radius. Aperture corrections were calculated for an infinite aperture and the instrumental magnitudes calibrated in the *HST* magnitude system (VEGAMAG) by adopting the zero-points listed in the WFPC 2 Data Handbook (Gonzaga & Biretta 2010). Saturated stars were measured in the short exposures and the resulting magnitudes properly rescaled for the exposure time. Owing to the considerable inefficiency with which charges are transferred in the WFPC 2 detectors, the magnitude of a star depends on its position on the detector and must, therefore, be corrected accordingly. To this aim, we have followed the prescriptions of Dolphin (2000).

Of the originally identified $\sim 8\,350$ stars in F814W, 78 % have a photometric uncertainty smaller than 0.1 mag. The fraction of stars with uncertainty on the magnitudes smaller than 0.1 mag is 67 % in F606W, 37 % in F450W, 7 % in F300W and 6 % in F656N. Following Romaniello et al. (2002), it is convenient to define the mean error of each star in the four broad-bands (δ_4) as:

$$\delta_4 = \sqrt{\frac{\delta_{300}^2 + \delta_{450}^2 + \delta_{606}^2 + \delta_{814}^2}{4}} \quad (6)$$

where δ_{300} , δ_{450} , δ_{606} and δ_{814} are the uncertainties in each individual band.¹ A total of $\sim 1\,300$ stars have a mean error $\delta_4 < 0.1$ mag and they all have broad-band magnitudes brighter than $m_{300} \simeq 23.5$, $m_{450} \simeq 23.9$, $m_{606} \simeq 23.2$ and $m_{814} \simeq 22.5$. The photometric completeness at these relatively bright magnitudes only depends on the stellar density and the presence of bright saturated stars. Since the average star-to-star distance at $m_{606} \simeq 23.2$ is ~ 22 pixel and the FWHM of the PSF is less than 2 pixel, the photometric completeness is very close to 100 %.

3 COLOUR–MAGNITUDE DIAGRAMS

In Figure 2 we show the colour–magnitude diagrams (CMDs) obtained by combining the data of all three WF chips in the broad-band filters. We show the CMDs corresponding to the most common colour combinations. Objects with an average photometric error $\delta_4 < 0.1$ are marked with thicker and darker dots. As indicated above, the inspection of Figure 1 already suggests the presence of patchy absorption. This is further confirmed by the CMDs of Figure 2, where for instance the upper stellar main sequence (MS) appears, in all colours, considerably broader than the photometric uncertainty typical of stars with $\delta_4 < 0.1$ mag. Some of the observed broadening can be caused by an age spread across the field, particularly in the upper MS (UMS) populated by B-type stars that evolve on a time-scale (few Myr) comparable with that of the star formation process itself (e.g. Iben 1974).

For reference, the lines plotted to the left of the MS in Figure 2b correspond, from left to right, to isochrones for a population with metallicity $Z = 0.008$ and ages of, respectively, 4, 20 and 40 Myr from the models of Marigo et al. (2008) for the specific WFPC 2 bands used here. For purposes of illustration, the isochrones have been reddened according to the Galactic extinction law, by an amount corresponding to $E(B - V) = 0.3$. This

¹ The definition given by Equation 6 can be generalized for any combination of bands. For instance, in Section 5 we will refer to the combined photometric uncertainty δ_3 in the *V* (F606W), *I* (F814W) and *H α* (F656N) bands.

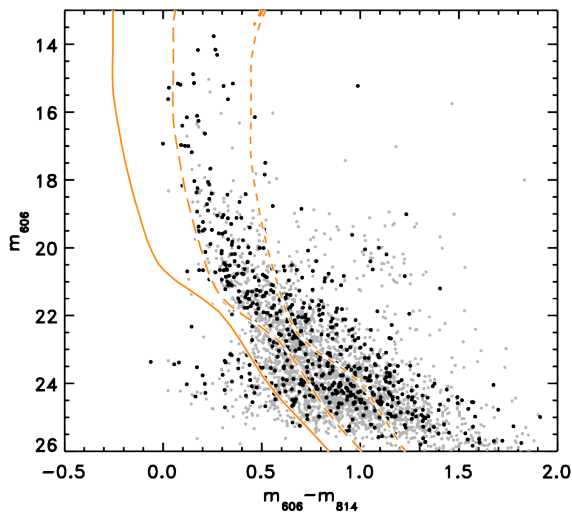


Figure 3. Same CMD as in Figure 2c but only for the stars inside the WF3 chip. Darker dots are used for stars located within 3 times the half-light radius of the small cluster near the lower-left corner of Figure 1. Light grey dots correspond to the rest of the stars in WF3. Isochrones from Marigo et al. (2008) for age of 4 Myr and three values of $E(B - V)$, namely 0, 0.3, and 0.7.

value includes the intervening MW absorption along the line of sight to the LMC, which accounts for $E(B - V) = 0.07$ or $A_V = 0.22$ (Fitzpatrick & Savage 1984). As for the distance, throughout this paper we will assume the distance modulus for the LMC as that of SN 1987A determined by Panagia (1998), namely $(m - M)_0 = 18.55$, corresponding to a distance of 51.4 kpc as mentioned above. While some of the colour spread at the brightest end can be caused by age, it appears that without a considerable spread in reddening it would be hard to justify the broadening observed at $m_{606} \lesssim 20$, where all stars have photometric uncertainty $\delta_4 < 0.1$.

Furthermore, strong indication of the presence of differential reddening on very small scales comes from the CMD of the stars belonging to the very compact cluster centred around the star identified as 05374631-6909100 in the 2MASS catalogue, located near the lower-left corner of Figure 1, in chip WF3. In Figure 3 we show the CMD of the whole of chip WF3 (grey dots) compared with that of the cluster stars (thick black dots), defined as those within three times the apparent cluster half-light radius of $5''$ or 1.2 pc. Since the cluster members are most likely coeval, the presence of considerable colour scatter in this small region suggests that the effects of differential extinction are significant.

As an initial attempt to estimate the range of extinction, we plot in Figure 3 the 4 Myr isochrone of Marigo et al. (2008) used in Figure 2 and apply to it a reddening correction according to the Galactic extinction law of Seaton (1979) for different values of $E(B - V)$. While there is no guarantee that the average Galactic extinction law applies in this region (in fact it does not, as we will show in Section 5), our purpose here is to show that CMDs are severely dominated by variable extinction. The solid, long-dashed and short-dashed lines correspond respectively to colour excess values of $E(B - V) = 0, 0.3$ and 0.7 . The largest majority of MS stars seem to lie in the colour range defined by $0.3 < E(B - V) < 0.7$, with very few of them bluer than the $E(B - V) = 0.3$ limit. The long-dashed line, defining the blue envelope to the observed MS,

can be considered as representative of the cluster’s zero-age MS. From it, we infer an approximate initial mass for the brightest stars at $m_{606} = 13.8$ of $\sim 40 M_\odot$. Unfortunately, a more precise mass (and age) determination would require an accurate knowledge of the reddening towards each star, which is not possible due to the lack of reference evolutionary features on the MS.

However, of particular interest for understanding the extent of patchy absorption and the ensuing differential reddening is the inspection of the elongated stellar sequence running almost parallel to the MS at $m_{606} \simeq 20$ in Figure 2 (easier to see in Panels b and c). This apparent sequence is in reality the clump of red giant stars (hereafter “red clump”, RC), characteristic of low-mass, metal-rich stars experiencing their He-burning phase and represents the counterpart at high metallicity and younger ages of the horizontal branch seen in CMDs of globular clusters. The RC usually appears as a very tight, well defined feature in the CMD of stellar populations. For instance, in the solar neighbourhood, *Hipparcos* data show the RC to extend in colour over the range $0.8 < (V - I)_0 < 1.25$, with a mean absolute magnitude $M_I = -0.23 \pm 0.03$ and a dispersion in magnitude of $\sigma_{RC} = 0.20$ mag (Stanek & Garnavich 1998). While this has suggested that the RC could in principle be used as a distance indicator (Paczynski & Stanek 1998), later theoretical works (e.g. Cole 1998; Girardi et al. 1998; Girardi & Salaris 2001; Salaris & Girardi 2002) have shown that this requires the knowledge of the properties of the population being studied, since metallicity and age affect the magnitude and colour, as well as the shape of the RC in the CMD.

Obviously, also the intervening absorption affects the location of the RC in the CMD. Recently, Nataf et al. (2013) have compared differences in the colour and apparent magnitude of RC stars towards several sight lines in the Galactic bulge to derive the extinction law in this part of the Galaxy. Extinction can even modify the apparent shape of the RC in the CMD if the absorption is patchy like in our case (Figure 1), since the amount of extinction varies from star to star and the RC becomes in practice an elongated feature (hereafter called “strip”) running parallel to the direction of the reddening vector. Fortunately, as we explain below, models show that age, metallicity, distance and reddening act differently on the location and the shape of the RC in the CMD. Therefore, with high precision and high resolution photometry of a large number of stars in four or more bands it is possible to disentangle the four effects and determine or constrain their values. In the sections that follow we will make use of this information to derive the extinction law in this specific region of the LMC and to measure absolute reddening towards individual stars.

We start by illustrating the method, which hinges on the central assumption that a single extinction law applies throughout this field. Note, however, that this is not just a mere assumption but rather an inference, since the existence of a well-defined reddening vector in each of the CMDs (see Figure 2) argues for one and the same extinction law for all the stars.

4 THE RED GIANT CLUMP

Girardi & Salaris (2001) and Salaris & Girardi (2002) have studied the behaviour of the mean RC as a function of age and metallicity. In particular, they have derived the average absolute magnitude and colour in the V and I bands from synthetic CMDs for different combinations of age and metallicity, as well as for different star formation histories. In their models, stars belonging to the RC are all those that have passed the He flash and are experiencing their central He burning phase (Cannon 1970). Using theoretical CMDs

of the same type, computed for the specific WFPC 2 bands of our observations, we have studied the shape of the RC.

The theoretical CMDs are based on the simple case of a single burst of star formation and a Salpeter initial mass function, starting from a set of isochrones and corresponding luminosity functions for various ages and metallicities. The grid of models covers ages in the range from 1.4 Gyr through to 3.0 Gyr with a step of 0.4 Gyr and four values of the metallicity, namely $Z = 0.001, 0.004, 0.008$ and 0.019 , i.e. roughly from $1/20 Z_{\odot}$ to Z_{\odot} . In fact, red clump stars can have ages up to 10 Gyr, but as illustrated by Girardi & Salaris (2001), the age distribution of red clump stars in galaxies with constant star formation is strongly skewed towards younger ages, due to the longer lifetimes of more massive RC stars and to the decreasing rate at which stars leave the MS at older ages. Moreover, red clump stars with ages between 3 and ~ 9 Gyr change very little their intrinsic positions in the CMDs. This justifies limiting our interval at ages up to 3 Gyr.

We have characterised the location of all RC stars in the corresponding CMDs by means of Hess diagrams, fitting a series of elliptical isophotes to the RC in each CMDs in order to determine its parameters, namely the colour, magnitude, semi-major axis, ellipticity and position angle. The essence of our simulations is shown schematically in Figure 4, where we plot the theoretical RC, for each combination of age and metallicity, in the plane of the CMDs defined by our bands. The age ranges from 1.4 to 3.0 Gyr and the metallicity from $Z = 0.001$ to 0.019 , as indicated. We have selected in all panels the $m_{450} - m_{606}$ colour, since it is similar to the commonly used $B - V$. All ellipses shown in the figure correspond to the 67% isophotal profile and therefore define the 1σ uncertainty. In order to convert absolute magnitudes to apparent values, we have assumed a distance modulus $(m - M)_V = 18.55$, as mentioned above, as appropriate for the neighbouring SN 1987A field in the LMC (Panagia 1998). The resulting magnitudes have been further corrected for the interstellar extinction component due to the MW along the line of sight to the LMC, corresponding to $E(B - V) = 0.07$ (Fitzpatrick & Savage 1984; see also Brunet et al. 1975 and Isserstedt 1975). The reddening corrections in the various bands amount to $A_{300} = 0.36$, $A_{450} = 0.26$, $A_{606} = 0.18$, and $A_{814} = 0.12$. Note that, at longer wavelengths, the differences between the magnitude of the RC at different ages and metallicity progressively decrease, as is witnessed by the shrinking scale in the ordinates from panel a) through to d).

Since both the distance and the MW foreground component of the extinction are fixed, the ellipses of Figure 4 can only move in the CMD because of the extinction within the LMC. As an example, the arrows plotted in Figure 4 show the reddening vector corresponding to the MW extinction law of Seaton (1979), for a colour excess $E(B - V) = 0.4$. Figure 4 is useful to understand the combined effect of metallicity, age and extinction on the location and shape of the RC in the CMD and can be directly compared with the observations to derive or constrain the properties of the population. This is particularly true when observations in several bands are available, since Figure 4 shows that metallicity, age and reddening affect the position of RC stars in different ways in the CMDs defined by our bands.

For instance, age does not appear to considerably affect the magnitude of the RC, except at very low metallicity. As for the reddening, in bands longwards of $\sim 4000 \text{ \AA}$ an increase of reddening or metallicity move the RC along very similar directions. While the reddening vector shown in Figure 4 follows the MW extinction law, namely $R_V = A_V/E(B - V) = 3.1$, the situation would not change if the slope of the extinction law would vary within a

factor of $\pm 30\%$ (i.e. $2 \lesssim R_V \lesssim 4$). Therefore, if the absolute value of the reddening is known and so is the distance, the position of the observed RC in these bands can constrain the metallicity of the population leaving some uncertainties on the age. Interestingly, this limited sensitivity of the RC to age and metallicity makes it easier to estimate the amount of reddening when there is considerable interstellar extinction ($A_V > 1$), since in this case the magnitude and colour displacement of the RC in the CMD due to extinction dominates over all uncertainties on metallicity and age. We will address this case specifically in Section 5. When observations at shorter wavelength are available (e.g. Figure 4a), it also becomes possible to break the degeneracy between reddening and metallicity. Provided that the distance is known, both the extinction law and reddening value A_V can be derived.

5 MEASURING THE EXTINCTION FOR RED CLUMP STARS

The theoretical location of the RC predicted by our simulations is shown together with the observations in Figure 5, from which some preliminary qualitative information on the old population present in this field can be drawn. The thick green circles show the position of the RC for an age of 2.2 Gyr and, from left to right, the two values of the metallicity defining the current range of accepted values for the LMC, namely $Z = 0.004$ and 0.008 (e.g. Hill, Andrievsky & Spite 1995; Geha et al. 1998). The choice of band combinations in the CMDs of Figure 5 always include the F814W band, since its photometry is most accurate. An inspection of Panels b) and c), where the photometric uncertainties are smaller, immediately reveals that age and metallicity alone cannot explain the elongated shape of the RC, which requires instead a large spread of reddening values to be reproduced. For comparison, the arrow corresponds to a reddening spread of $E(B - V) = 0.4$, for the Galactic extinction law, but the extension of the RC suggests that the actual spread is even higher.

Given this considerable range of extinction values, the CMD in Panel a) suggests that the metallicity of the population is not likely to extend beyond the $0.004 < Z < 0.008$ range, since this would require a colour spread larger than observed for RC stars. This is consistent with the average metallicity of field stars in the LMC being $Z \simeq 0.007$ (e.g. Hill, Andrievsky & Spite 1995; Geha et al. 1998), but it confirms that large spreads may exist and that lower metallicity stars are likely present in this region (according to Dopita et al. 1997 the LMC metallicity might have almost doubled over the past 2 Gyr). As regards the age of RC stars, comparison between the observations and models in Panel c) suggests that it is most likely in excess of 1 Gyr, given the limited magnitude spread of the RC band.

In order to proceed to a more quantitative analysis of interstellar extinction in this field, it is necessary to determine more precisely which stars belong to the RC and to calculate their displacement in the CMD from the location that they would occupy if there were no extinction. For a starting location, which we hereafter will call “nominal RC”, we take the theoretical RC of stars of the lowest metallicity consistent with the data, in the sense that for all ages in our range of models the nominal RC should not be redder than the observed RC stars, in all bands simultaneously. In the case of our field, Figure 5 suggests that the most appropriate metallicity is $Z = 0.004$. This choice defines in practice the magnitude of the nominal RC, given the limited spread in luminosity within each metallicity class (see Figure 4c). As for its colour, we take it to be

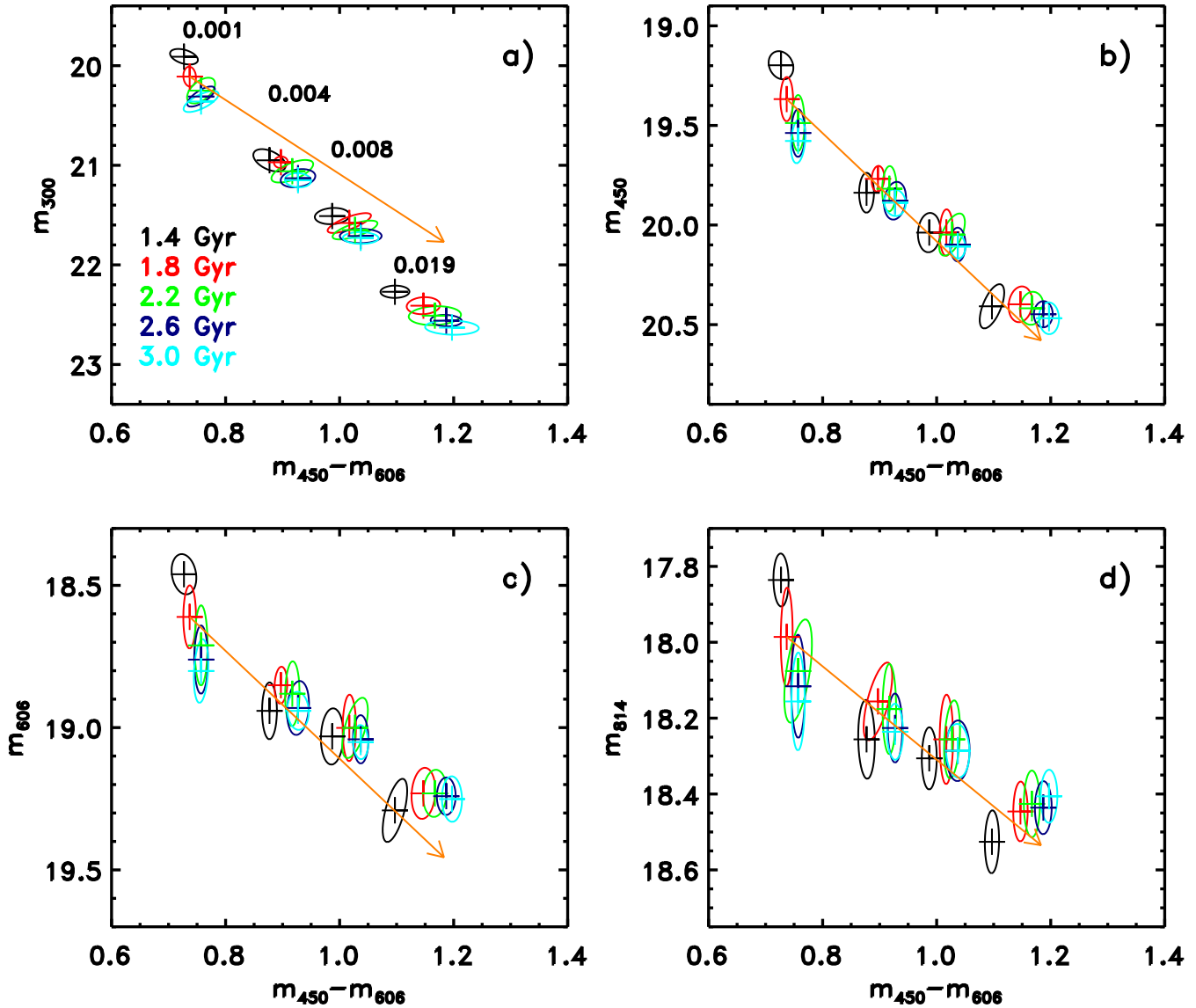


Figure 4. Red clump nominal ellipses from the models of Girardi & Salaris (2001) for various ages and metallicities, as indicated. The ellipses correspond to the 67% isophotal profile measured in the Hess diagrams. A distance modulus of 18.55 is assumed and account is taken of the interstellar extinction component due to the MW along the line of sight to the LMC, corresponding to $E(B - V) = 0.07$. The shrinking scale in the ordinates from Panel a) through to d) shows that the magnitude differences progressively decrease at longer wavelengths. For illustration purposes, the arrow shows the reddening vector corresponding to $E(B - V) = 0.4$ for the MW extinction law.

the average RC colour for ages in the range 1.4 – 3.0 Gyr, since lower ages are less likely as Figure 5a shows.

As for the uncertainties on the nominal RC colour and magnitude, we have taken the uncertainties at each age for $Z = 0.004$ and combined them in quadrature. The corresponding magnitudes, already including the effects of intervening MW extinction, are $m_{300} = 21.11 \pm 0.12$ and $m_{450} = 19.81 \pm 0.12$, $m_{606} = 18.89 \pm 0.09$, $m_{814} = 18.21 \pm 0.10$, and the colours in the most common band combinations are $m_{300} - m_{450} = 1.3 \pm 0.1$, $m_{450} - m_{606} = 0.92 \pm 0.06$ and $m_{606} - m_{814} = 0.68 \pm 0.04$, with all uncertainties given at the 1σ level. The resulting nominal RC, defined in this way, is shown as an example by the ellipse in Figure 6 in the m_{606} vs. $m_{606} - m_{814}$ CMD, where photometric uncertainties are smallest. The semi-major and semi-minor axes of the ellipse are, respectively, 2.5 times the uncertainty on the RC magnitude and colour.

© 2013 RAS, MNRAS 000, ??–??

5.1 Identifying red clump stars

The first condition to be met by true RC stars in the CMDs of Figure 6 is that they must be redder and fainter than the nominal RC ellipse. We begin by considering as candidate RC stars all objects redder than the MS by at least three times its colour width. The dashed line shows the MS ridge line, determined by iteratively removing from each magnitude bin all stars with a colour departing by more than 2.5σ from the median. The solid curve corresponds to the 3σ envelope and we consider as candidate RC stars all objects redder than this curve.

The effect of differential extinction is to spread the stars contained in the nominal RC ellipse throughout the CMD, according to the extinction law, thus forming a strip of higher stellar density. Also red giant stars brighter and fainter than those in the RC are displaced by reddening in the CMD plane and must be excluded

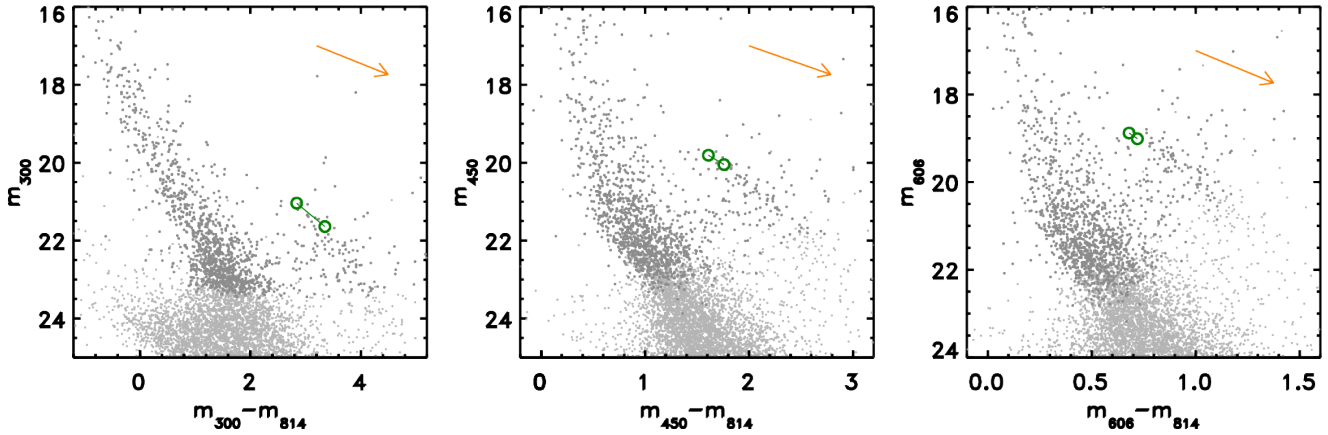


Figure 5. The CMD of the stars in our field is compared with the theoretical positions of the RC for metallicity $Z = 0.004$ and 0.008 (left and right, respectively), having assumed a distance modulus $(m - M)_V = 18.55$ and a MW contribution to the extinction along the line of sight of $E(B - V) = 0.07$. For illustration purposes, the arrows show the reddening vector for the MW extinction law with $E(B - V) = 0.4$.

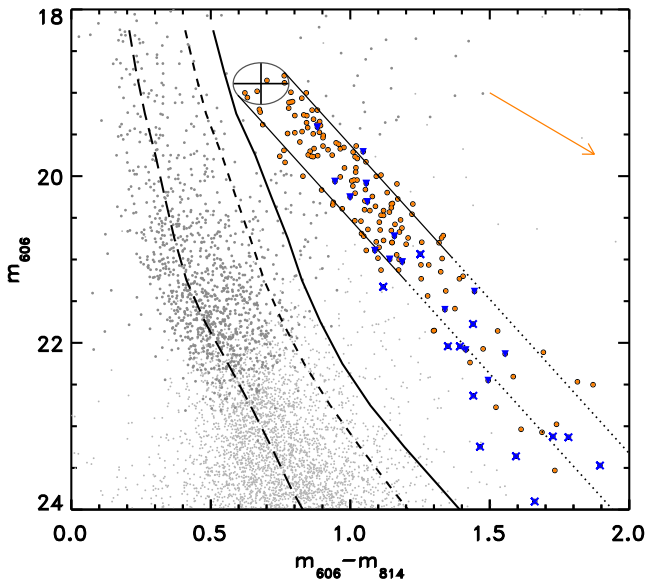


Figure 6. The nominal position of the RC, already including the effects of MW reddening, is shown by the ellipse. To select reddened RC stars we have excluded all objects bluer than the solid line, which are closer to the MS ridge line (dashed line) than three times the width of its colour distribution (3σ). Thick orange dots inside the region marked by the solid straight lines are candidate RC stars, whereas objects indicated with crosses or triangles are likely PMS objects, which we have excluded from our sample. As in Figures 4 and 5, the arrow shows the reddening vector for the MW extinction law, with $E(B - V) = 0.4$.

from our analysis. However, if the extinction law is uniform (i.e. the same or very similar $A_\lambda/E(B - V)$ ratio applies to all objects in the field), only limited flaring is expected along the RC strip, which remains separate from other RG stars. This is easiest to see in the m_{606} vs. $m_{606} - m_{814}$ CMD of Figure 6, because photometric errors are small and, as Figure 4 suggests, the effect of reddening dominates.

As a first attempt to isolate bona fide RC stars, we trace two parallel lines, tangent to the ellipse and flanking the RC “beam” (shown by the lines tangent to the ellipse in Figure 6) and count the

number of stars contained within the area delimited by these lines, by the nominal RC ellipse at the left-hand side and by the condition $m_{606} - m_{814} \leq 2$ at the right-hand side, as a function of the lines slope. Stars falling outside of the beam by more than 2.5 times their colour and magnitude uncertainties are excluded. All stars indicated by thicker marks (dots, triangles and crosses) are candidate RC objects, although as we will show later we will limit the selection to stars corresponding to the dots brighter than $V \simeq 23.5$ (inside the region defined by the solid straight lines), to include only stars with photometric uncertainty on the m_{300} magnitude of less than 0.4 mag and excluding any objects indicated with triangles or crosses as they might be pre-main sequence (PMS) stars.

The number of stars inside the beam is shown in Figure 7 as a function of the slope. The slope that maximises the number of stars within the beam (used to draw the lines in Figure 6) gives a first indication of the extinction law in the form of the ratio $A_{606}/E(m_{606} - m_{814})$. With this choice of the slope, we find a total of 170 over the entire magnitude range, which we consider as candidate RC stars. All stars indicated by thicker marks in Figure 6 (i.e. dots, triangles and crosses) are candidate RC objects, although as we will show later we will limit the selection to stars corresponding to the dots brighter than $V \simeq 23.5$, since objects indicated with triangles and crosses might be PMS stars.

After this initial selection of RC candidates, the procedure to arrive at the final selection of bona fide RC stars, and at the determination of the reddening slopes in the CMDs, is as follows.

(i) We consider all CMDs in which the magnitudes of the stars are plotted as a function of the $m_{450} - m_{606}$ and $m_{606} - m_{814}$ colours, for a total of 8 different CMDs. An example is shown in Figure 8.

(ii) In each CMD we derive the best linear fit to the distribution of the 170 candidate objects, taking into account: 1) the uncertainties on their magnitudes and colours; 2) the uncertainties on the ellipse defining the model RC in each individual CMD; and 3) an equal number ($= 170$) of synthetic unreddened RC stars with a Gaussian distribution inside the ellipses. The latter step guarantees that the best linear fit passes through the centre of the nominal RC. We derive in this way the slope q of the best fit in each CMD, and the corresponding uncertainties σ_q .

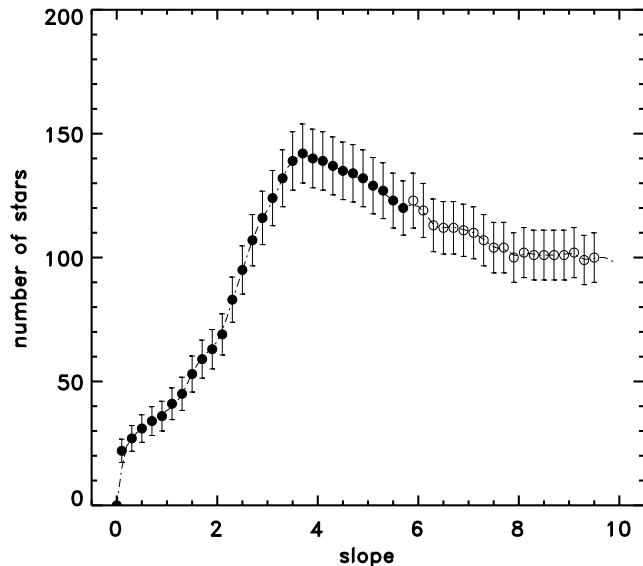


Figure 7. Number of stars contained within the RC “beam” as a function of the beam’s slope. This is used to show the slopes corresponding to the peak and minimum of the distribution. This is only done for the CMD in the F606W and F814W bands.

Table 2. Measured values of the ratio R between absolute (A) and selective (E) extinction in the specific bands of our observations, with corresponding uncertainties. The effective wavelength (λ) and wavenumber ($1/\lambda$) of each band are also indicated.

Band combination	R	λ [\AA]	μm^{-1}
$A_{300}/E(m_{450} - m_{606})$	5.19 ± 0.35	2979	3.36
$A_{300}/E(m_{606} - m_{814})$	5.51 ± 0.28	2979	3.36
$A_{450}/E(m_{450} - m_{606})$	4.70 ± 0.31	4531	2.21
$A_{450}/E(m_{606} - m_{814})$	5.05 ± 0.35	4531	2.21
$A_{606}/E(m_{450} - m_{606})$	3.79 ± 0.26	5938	1.68
$A_{606}/E(m_{606} - m_{814})$	4.03 ± 0.29	5938	1.68
$A_{814}/E(m_{450} - m_{606})$	2.88 ± 0.21	7942	1.26
$A_{814}/E(m_{606} - m_{814})$	3.11 ± 0.24	7942	1.26

(iii) In each CMD, we identify all objects inside the region defined by the nominal RC ellipse and two lines tangent to it having slopes corresponding to $q \pm \sigma_q$, and consider all stars with $\delta_4 < 0.15$ inside it (or $\delta_4 < 0.23$ for a coarser selection). We include also objects formally outside of this region but whose photometric error ellipses in the CMD would in part overlap with it.

(iv) The selection of objects identified in the previous step is further reduced by considering only objects whose m_{300} magnitude uncertainty is less than 0.4 mag. This reduces the sample to 107 bona-fide RC stars with $\delta_4 < 0.23$ (or 90 bona-fide RC objects with $\delta_4 < 0.15$).

(v) Finally, the procedure in step (ii) above is repeated on the bona-fide RC stars selected in this way in order to derive the slopes and uncertainties of the best fits in all bands, as shown for instance in Figure 7.

The reddening slopes derived in this way correspond to the value of the ratio R between absolute and selective extinction in the specific bands of our observations. The values of the ratio R and the corresponding uncertainties as are listed in Table 2.

5.2 Possible interlopers

An important step in assembling a reliable sample of bona-fide RC stars is the exclusion of interlopers. The latter are objects whose colours and magnitudes would place them inside the RC strip without their necessarily being sources of this type. An obvious class of possible contaminants is PMS stars, which in light of their younger age are systematically redder and brighter than MS objects. In their study of PMS stars in 30 Dor, De Marchi et al. (2011b) specifically excluded the region of the CMD where PMS and RC objects would overlap. In order to keep our sample of RC stars as much as possible free from PMS objects we have looked for stars with $H\alpha$ excess emission, which is a characteristic signature of accreting PMS stars.

Employing the method developed by De Marchi et al. (2010; 2011a) in order to identify stars with $H\alpha$ excess emission, we have compared the $V - H\alpha$ colours of all stars in the RC strip with those of all other stars in the field, as a function of their $V - I$ colours. The majority of stars in the field do not have $H\alpha$ excess emission. By selecting those with smallest combined photometric uncertainty in the V , I and $H\alpha$ bands ($\delta_3 < 0.05$, see Equation 6), we have derived the reference template providing the $V - H\alpha$ colour of non-emitting stars as a function of their $V - I$ colours. Any excess in $V - H\alpha$ with respect to the reference template can be converted into the corresponding equivalent width $W_{\text{eq}}(H\alpha)$ using the relationships provided in De Marchi et al. (2010).

Chromospheric activity is a likely source of $H\alpha$ emission in low-mass stars, due to non-radiative heating mechanisms powered by magnetic fields. In the outer layers of these stars the temperature increases towards the surface and the main cooling mechanism is radiative loss through strong resonance lines, such as indeed $H\alpha$ (e.g. Linsky 1980). Therefore, it is not surprising if some of the RC stars in our sample show $H\alpha$ excess emission from chromospheric activity. However, for objects of spectral type earlier than M the value of $W_{\text{eq}}(H\alpha)$ vis not expected to exceed a few \AA and if larger values are measured mass accretion must be present. Martin (1998) and more recently White & Basri (2003) have proposed thresholds above which stars with $H\alpha$ excess emission should be considered classical T Tauri objects. More precisely, as regard the spectral range applicable to our RC sources, White & Basri (2003) propose thresholds of 3\AA for stars of spectral type K 0 – K 5 and values larger than 10\AA for K 7 – M 2.5 stars.

We cannot assign an accurate spectral type or effective temperature to our objects, since we do not know their individual reddening values, but we can assume a typical reddening. We take $E(B - V) \simeq 0.2$, as this is the value given by Panagia et al. (1987) and Scuderi et al. (1996) for the region around SN 1987A and which, as we will see in Section 6, is also the average value for our region. In this case, almost all stars in the RC strip would have spectral type earlier than M 2.5, as they would have $(V - I)_0 < 1.5$, and those with $(V - I)_0 < 1$ would have spectral type K 5 or earlier. In Figure 6 we have indicated with crosses all stars with $10 \text{\AA} < W_{\text{eq}}(H\alpha) < 30 \text{\AA}$ and with triangles those with $3 \text{\AA} < W_{\text{eq}}(H\alpha) < 10 \text{\AA}$.

The former must be excluded from our sample as they are likely PMS stars and do not belong to the bona-fide RC population. Interestingly, they represent about 1/3 of the candidate objects in the RC strip with $V - I \gtrsim 1.3$, in the portion of the strip defined by the dotted lines in Figure 6. In fact, all these objects have already been excluded from our sample since they all have uncertainties in the m_{300} magnitudes exceeding 0.4 mag, as discussed above. However, as mentioned above there are also two objects with $W_{\text{eq}}(H\alpha) > 10 \text{\AA}$ in the sample of 107 bona-fide RC stars

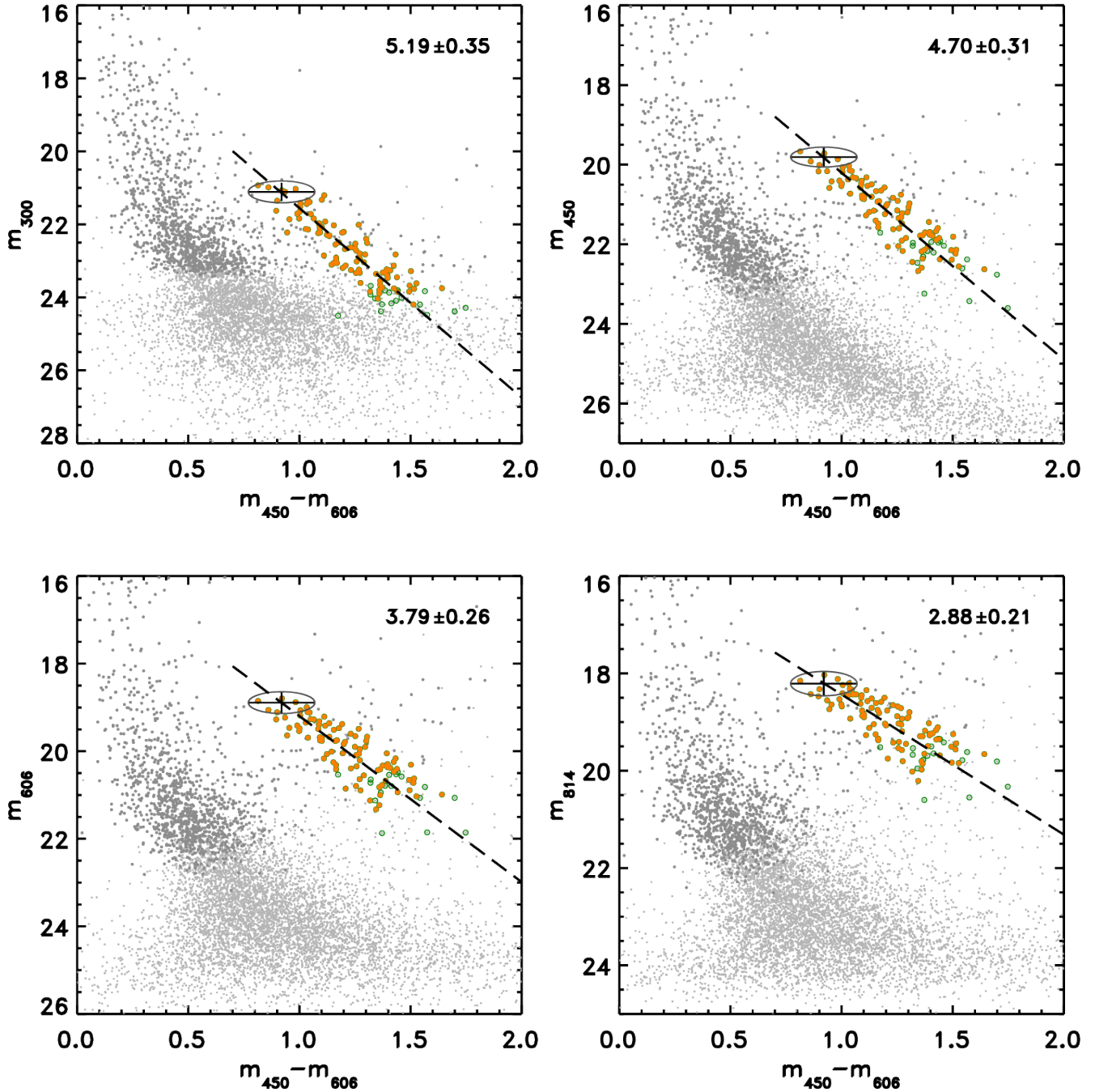


Figure 8. Bona fide RC stars. The thick orange dots are the 90 RC stars selected with a stricter $\delta_4 < 0.15$ condition, whereas the green circles are those with $0.15 < \delta_4 < 0.23$. The best fitting slopes and their uncertainties indicated in each panel refer to the 90 RC objects with stricter condition $\delta_4 < 0.15$.

with $\delta_4 < 0.23$ (respectively with $W_{\text{eq}}(H\alpha)$ of 14 \AA and 27 \AA), which we will remove as they too are likely PMS stars not related with the RC sample.

As for the stars with $3 \text{ \AA} < W_{\text{eq}}(H\alpha) < 10 \text{ \AA}$ (triangles), we have removed 10 of them from the same sample, since some might be PMS stars. However, these objects represent less than 10% of the total population and, more importantly, their placement inside the RC strip does not reveal any peculiarity in colour or magnitude distribution, compared with those of the objects with no $H\alpha$ excess.

This means that their presence would anyhow not affect the determination of the slope of the reddening vector that we derive in the following section.

5.3 Extinction law

As mentioned in the Introduction, it is customary to express the extinction law in the form of the ratio

$$R_\lambda \equiv \frac{A_\lambda}{E(B-V)}, \quad (7)$$

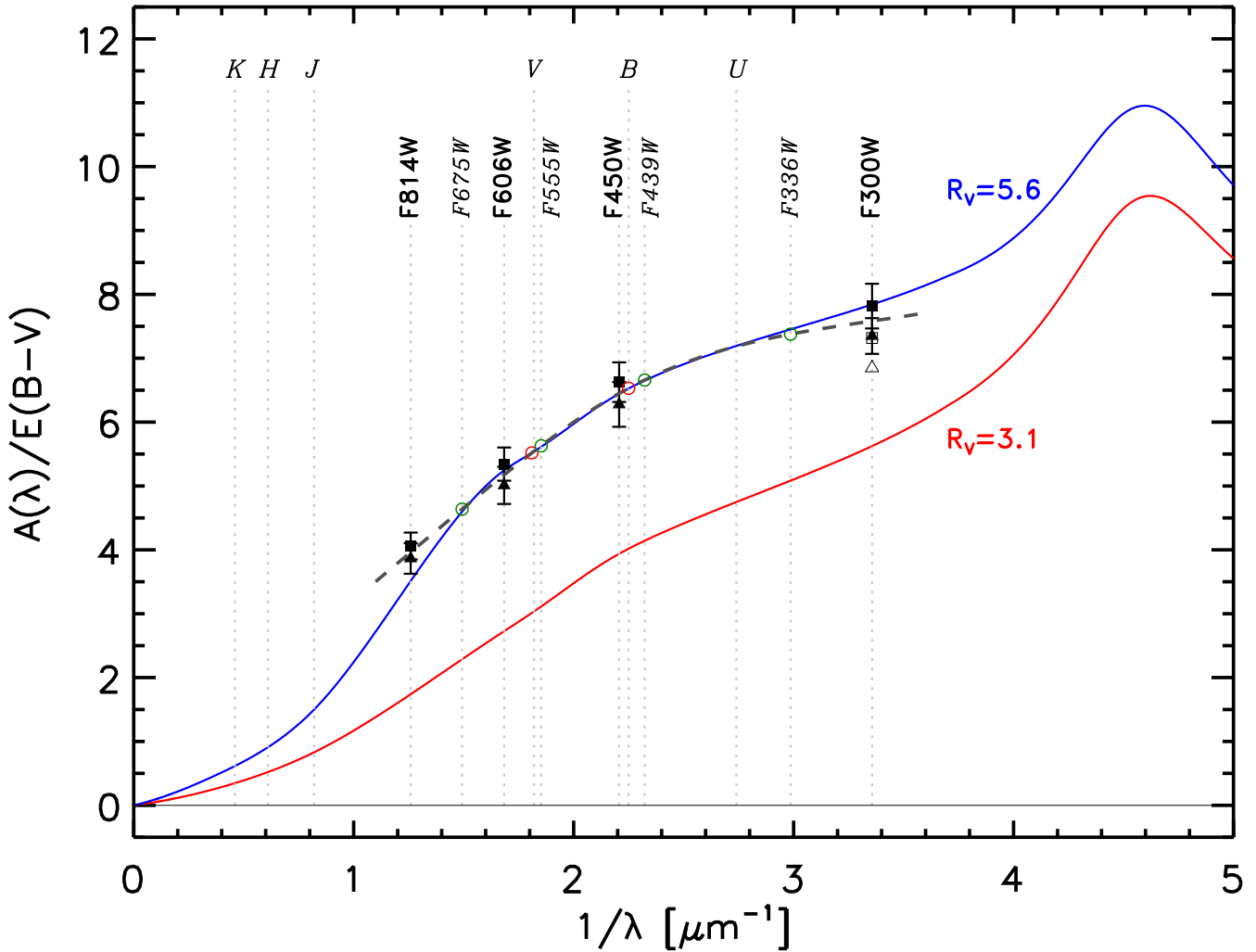


Figure 9. Extinction law. The dashed line is a spline interpolations through our measurements, with the filled squares representing those derived from the CMDs as a function of $m_{450} - m_{606}$ and filled triangles for the CMDs as a function of $m_{606} - m_{814}$. The circles are the interpolated values for the other WFPC 2 bands and for the Johnson B and V filters. The extinction law is in good agreement, within the uncertainties, with the parametric law of Fitzpatrick & Massa (1999) for $R_V = 5.6$ and is considerably shallower than the canonical Galactic extinction law ($R_V = 3.1$).

where A_λ is the extinction at the specific wavelength or band considered and $E(B - V)$ the colour excess in Johnson's B and V bands. The R values listed in Table 2 are expressed as a function of the colour excess in the specific WFPC 2 bands used in our observations. However, spline interpolation through the values listed in Table 2 allows us to derive A_B and A_V as a function of $E(m_{450} - m_{606})$ and $E(m_{606} - m_{814})$. We find $A_B/E(m_{450} - m_{606}) = 4.75$, $A_V/E(m_{450} - m_{606}) = 4.04$, $A_B/E(m_{606} - m_{814}) = 4.30$, and $A_V/E(m_{606} - m_{814}) = 5.11$. Taking into account that Equation 7 implies that $R_B - R_V = 1$, we can translate the values of Table 2 into the corresponding values as a function of $E(B - V)$. The values of R_λ found in this way are listed in Table 3 and shown graphically in Figure 9, where filled squares and filled triangles correspond to values obtained from measurements in the planes as a function of $m_{450} - m_{606}$ and $m_{606} - m_{814}$ colours, respectively. Within the uncertainties, the two sets of values are in excellent agreement with one another.

Note that for the F300W band it is necessary to take into account the considerable red-leak affecting magnitudes measured in this band (Lim et al. 2009). Reddened stars appear less attenuated

than they would be without red-leak because the filter allows some of the flux at longer wavelengths (6 000 – 10 000 Å) to pass. For a given star, the magnitude difference between F300W and an otherwise identical filter with no transmission above 5 000 Å depends on the extinction law and on the effective temperature of the star, being stronger for a shallower extinction curve (larger R_V value) and for cooler stars. To quantify this effect, we have used the *HST* synthetic photometry simulator *Synphot* (Laidler et al. 2005) to compare the expected magnitude of a red giant star of $T_{\text{eff}} = 5\,250$ K in the F300W band and in a band identical to it but with no transmission above 5 000 Å. The magnitudes were calculated for different values of $E(B - V)$, having assumed the extinction curve of Fitzpatrick & Massa (1999; in turn based on the original parametrization of Cardelli et al. 1989) for a value of $R_V = 5.6$, since this is the value suggested for this field by the other bands in our study (see below). We found in this way that the value of $A_{300}/E(B - V) \simeq 7.1$ that we measure (empty square and triangle in Figure 9, see also Table 3) would in fact be ~ 7.6 if the F300W band had no red-leak.

The dashed line in Figure 9 is a spline interpolation through the R_λ values obtained from our analysis (see Table 3) and it

Table 3. Measured and interpolated (*italics*) values of R_λ for various bands. The effective wavelengths (λ) and wave numbers ($1/\lambda$) of each band are also indicated. Note that all interpolated values, shown in *italics*, are given for the specific monochromatic effective wavelength indicated without considering the width of the filter. The R_λ value in the F300W band is corrected for the effects of red leak, as explained in the text.

Band	R_λ	λ [Å]	$1/\lambda$ [μm^{-1}]
F300W	7.58 ± 0.33	2979	3.36
F336W	<i>7.38</i>	3349	2.99
U	<i>7.19</i>	3650	2.74
F439W	<i>6.66</i>	4305	2.32
B	<i>6.52</i>	4450	2.25
F450W	6.45 ± 0.25	4531	2.21
F555W	<i>5.63</i>	5398	1.86
V	<i>5.53</i>	5510	1.82
F606W	5.18 ± 0.24	5938	1.68
F675W	<i>4.64</i>	6697	1.49
F814W	3.96 ± 0.14	7942	1.26
J	<i>1.50</i>	12200	0.82
H	<i>0.92</i>	16300	0.61
K	<i>0.61</i>	21900	0.46

agrees, within the uncertainties, with the extinction law of Fitzpatrick & Massa (1999) for a value of $R_V = 5.6$. In Table 3 we give the values of R_λ at the effective wavelengths of a number of *HST* and standard photometric bands. The wavelengths are also shown graphically by the vertical dotted lines in Figure 9.

With $R_V = 5.6$, the extinction law for this field is considerably less steep than the canonical Galactic extinction law, with $R_V = 3.1$, which is also shown in Figure 9. The R_V value that we find is also considerably less steep than those reported by Gordon et al. (2003) in the LMC. These authors combined observations with the *International Ultraviolet Explorer* (discussed in Fitzpatrick & Massa 1990), and photometry from ground-based facilities at optical and infrared wavelengths, to derive the extinction law towards 19 sight lines in the LMC, from UV to near-infrared wavelengths. Note that, in order to determine the absolute extinction from the measured colour excess, Gordon et al. (2003) adopted the customary approximation $R_V = 1.1 \times E(V - K)/E(B - V)$, which is reliably valid only for $R_V \simeq 3$ (Bouchet et al. 1985; Fitzpatrick & Massa 2007). The average R_V value that they find for eight stars in the LMC 2 supershell near the 30 Dor star formation region is 2.76 ± 0.09 , while the average over ten other LMC lines of sight gives a higher value, $R_V = 3.41 \pm 0.06$.

Our larger R_V value corresponds to a “flatter” extinction law, which in turn implies that the dust grains size distribution is skewed towards larger grains, compared with the canonical average Galactic extinction law in the diffuse interstellar medium (e.g. Cardelli et al. 1989; Kim, Martin & Hendry 1994). Put differently, this implies that larger grains dominate (e.g. van de Hulst 1957). At optical wavelengths the extinction curve that we find follows closely the Galactic curve, with a grey offset of about 2.5. This offset indicates the presence of grains relatively large, with sizes roughly of the order of $\lambda/(2\pi)$. A large R_V value appears to be typical of denser environments (e.g. Johnson & Borgman 1963; Cardelli et al. 1989; Weingartner & Draine 2001 and references therein) and this could suggest that a denser environment favours either a more efficient formation of larger grains or the survival of larger grains to the detriment of the smaller ones.

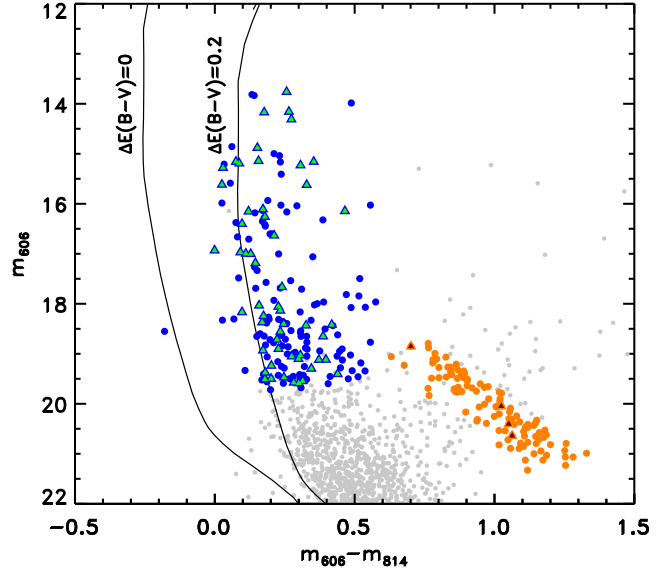


Figure 10. The stars indicated by thick dots are used to study the distribution of reddening in the field. Triangles correspond to stars located inside a radius of $15''$ (3.75 pc) of the small young cluster in the field. The left-hand curve is the 4 Myr old isochrone with only MW extinction, namely $E(B - V) = 0.07$, applied to it, while the solid curve on the right also includes an additional $\Delta E(B - V) = 0.2$ applied according to the extinction law derived in this work.

Thus, it is possible that this region is simply denser than those probed by the individual lines of sight sampled by Gordon et al. (2003) and, therefore, the $R_V = 5.6$ value that we find might be characteristic of just this region. More in general, it could be the result of systematically different conditions of the environment in the LMC, compared to the MW. We will address this issue in a series of forthcoming papers (De Marchi & Panagia in preparation) devoted to the reddening distribution in the centre of the 30 Dor region, as well as in the area surrounding it. Recent high-quality *HST* observations exist in for these regions at UV, optical and near-infrared wavelengths and they reveal a prominent extended RC in the CMDs (De Marchi et al. 2011b; Sabbi et al. 2013). These observations cover also the *J* and *H* bands, which will allow us to measure the properties of the extinction law in the near infra-red and to further validate the $R_V = 5.6$ value obtained in this work.

6 REDDENING DISTRIBUTION

Having derived the extinction law applicable to the stars in this field, it is possible to measure the extinction towards individual objects when the nominal location of these stars in the CMD can be accurately determined, like in the case of RC stars. We will consider separately RC objects and stars in the UMS, in order to study the relative distribution of stars and dust in this field. Using data from the Magellanic Clouds Photometric Survey (Harris, Zaritsky & Thompson 1997), Zaritsky (1999) concluded that there is a significant difference in the extinction towards hot ($T_{\text{eff}} > 12000$ K) and cold ($5500 \text{ K} < T_{\text{eff}} < 6500$ K) stars, with the hotter stars being more highly extinguished on average. As we will show, this conclusion does not apply to the objects in this specific field.

The objects that we consider in this study are indicated as thick symbols in Figure 10. Besides the bona-fide RC stars discussed in the previous section, we have also considered all UMS stars that

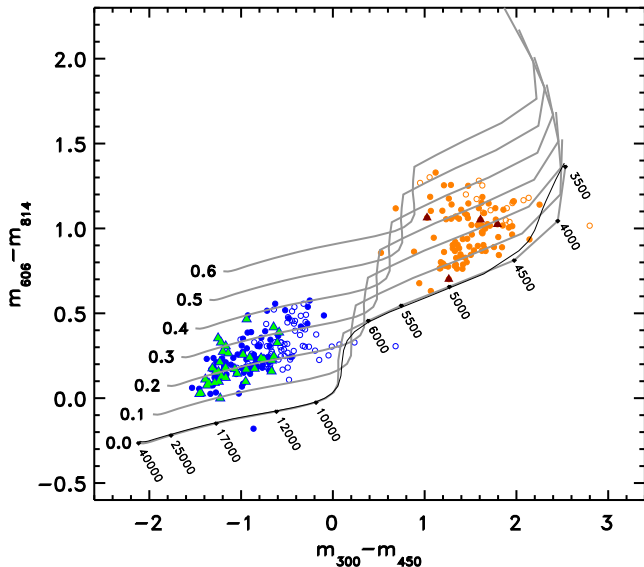


Figure 11. Colour–colour diagram for all the stars shown as thick symbols in Figure 10. The symbols (and colours) are the same. The stars shown with unfilled dots are objects with larger photometric uncertainty ($\delta_4 < 0.23$ instead of $\delta_4 < 0.15$). The solid lines show the colours of the model atmospheres of Bessell et al. (1998), to which we have applied incremental reddening as per the $E(B - V)$ values indicated next to each curve, according to the extinction law that we have derived in Figure 9.

are brighter than the 20th magnitude in all four bands. Objects indicated by triangles are those within a radius of 15'' (3.75 pc) from the centre of the small young cluster in the field (see Figure 1). They represent 1/3 of the UMS objects in the field, although four RC stars are projected in the same area. Also shown in Figure 10 is the isochrone for a population with metallicity $Z = 0.008$ and age of 4 Myr from the models of Marigo et al. (2008). The isochrones are shown for two values of the reddening: the one on the left only includes the intervening MW absorption along the line of sight to the LMC, namely $E(B - V) = 0.07$ as mentioned above, without any additional LMC reddening, while the one on the right has an additional reddening $\Delta E(B - V) = 0.2$, applied according to the extinction law derived in the previous section.²

We derive the reddening towards each of the selected UMS and RC stars from the colour–colour (CC) diagram of Figure 11, in order to make full use of the measurements in four bands available for all of them. The thick ‘‘S’’-shaped solid line at the bottom of the figure corresponds to the theoretical colours from the models of Bessell, Castelli & Plez (1998) for stars with gravity $\log g = 4.5$, metallicity $Z = 0.006$ and effective temperature in the range 3 500 K – 40 000 K, for the specific WFPC2 photometric bands used in this work (see also Romaniello et al. 2002). It already includes the MW contribution to the reddening along the line of sight. For comparison, we also show as a thin line the colours corresponding to the 4 Myr old isochrone of Marigo et al. (2008) for $Z = 0.008$, also including the MW contribution to the reddening. Except for the lowest temperature range, which is outside of our region of interest, the two sets of models match each other very closely.

Note that, due to the value of the surface gravity adopted for

² Hereafter, we indicate with $\Delta E(B - V)$ the reddening in addition to the contribution of the MW along the line of sight to the LMC.

the Bessell et al. (1998) models, the latter are in principle only suitable to MS stars. However, Romaniello et al. (2002) have convincingly shown that they can be effectively used also for RG stars, since the effect of a lower surface gravity on objects with $T_{\text{eff}} \lesssim 5\,500$ K is negligible. Furthermore, the validity of these models in the WFPC2 bands used here has been specifically addressed by Romaniello et al. (2006).

Our goal is to derive information on the interstellar reddening by comparing the colours of the observed stars with those of the models. Since the ratio of the colour excesses in different bands is set by the extinction law that we derived in the previous sections, the displacement of the S-curve in the CC plane must take place accordingly. At first sight it may then seem sufficient to shift solidly the bottom S-curve along both axes of the CC diagram, according to the extinction law, until the models agree with the data. However, although R_λ is fixed by the extinction law at a given wavelength, the extinction value A_λ corresponding to a given $E(B - V)$, once averaged over the bandwidth, depends on the temperature of the star. This is due to the non negligible bandwidth of the filters causing the effective extinction in a band to depend on the shape of the spectrum, which in turn is a function of the star’s temperature. As Romaniello et al. (2002) and Girardi et al. (2008) have shown, this effect is more pronounced for cold stars than for hot stars and for blue filters than for red filters.

This implies that reddening not only moves the S-curve to the right and upward in the CC plane, but it also modifies its shape at redder colours, making it steeper, i.e. more curved. This can be seen in Figure 11, where the lowest thick grey curve corresponds to the models of Bessell et al. (1998), to which we have already applied the attenuation corresponding to the Galactic extinction along the line of sight to the LMC. The other thick grey curves represent the same models, to which we have further applied an attenuation corresponding to incremental values of $E(B - V)$, assuming the extinction specific to this region as derived in the previous section. In practice, since the parametric description of Fitzpatrick & Massa (1999) with $R_V = 5.6$ agrees very well with our extinction law (see Figure 9), we have used it to calculate the attenuation of the model atmospheres over the entire wavelength range covered by the models, for values of $\Delta E(B - V)$ ranging from 0 to 1 in steps of 0.01 mag. Using *Synphot* (Laidler et al. 2005), we have folded the models attenuated in this way through the specific WFPC 2 bands and derived the corresponding magnitudes in the *HST* system. The thick solid lines in Figure 11 correspond to values of $\Delta E(B - V)$ ranging from 0 to 0.6 in steps of 0.1, as indicated.

Comparing the distribution of UMS and RC stars in the figure reveals that the former span a narrower range of $\Delta E(B - V)$ values and in particular the UMS stars in the small cluster (triangle) have the narrowest range. Conversely, RC stars are distributed over a wider range of $\Delta E(B - V)$, extending both to lower and higher values. This can be seen more easily in Figure 12, showing the histograms of the distribution of RC stars (solid line), the UMS stars inside the small cluster (short-dashed line) and the UMS elsewhere in the field (long-dashed line). The spread in the $\Delta E(B - V)$ values of UMS stars is possibly slightly overestimated, since some of it can be due to stellar evolution. In other words, an age difference of a few Myr can imply a significant colour difference in the CMD for UMS stars (see e.g. Figure 11), whereas for RC stars the dominant cause of the spread observed in the CMD is reddening, as discussed in Section 4.

The spatial scale of the extinction variations is illustrated in Figure 13, which shows a map of the $\Delta E(B - V)$ values towards the RC (orange dots) and UMS (blue dots) in the sample. The ori-

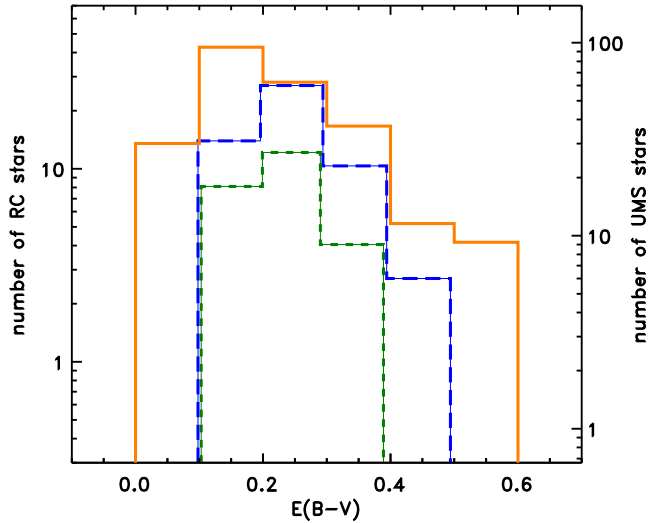


Figure 12. Histograms of the number of RC and UMS stars. The solid line (orange in the online version) gives the number of RC stars, according to the ordinates at left. The reddening distribution of UMS stars is indicated by the dashed lines: the short-dashed line (green in the online version) is for the stars in the small cluster, while the long-dashed line (dark blue in the online version) is for all other UMS stars in the field. The number of UMS stars is given by the ordinates at right.

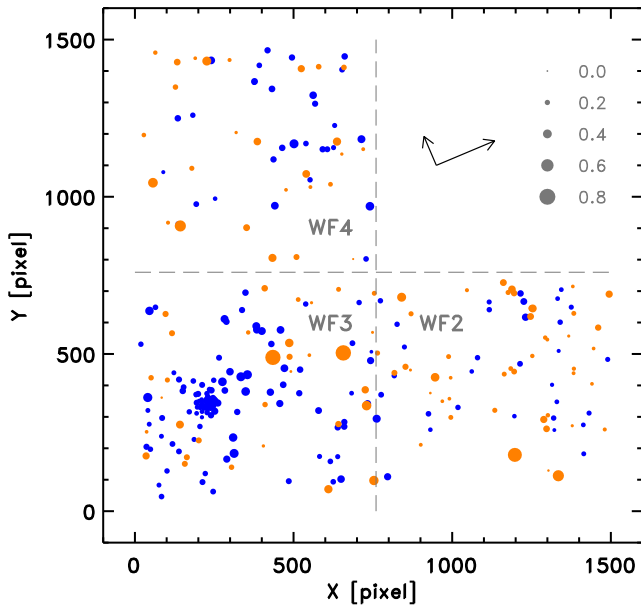


Figure 13. Map of the measured $\Delta E(B - V)$ values towards the RC stars (orange dots) and UMS stars (blue dots) in the sample. The orientation is the same as in Figure 1 and the size of the symbols is proportional to the $\Delta E(B - V)$ value, as per the legend. Each pixel corresponds to $0''.1$.

entation is the same as in Figure 1 and the size of the symbols is proportional to the $\Delta E(B - V)$ value, as per the legend. The values of the minimum, maximum, average and standard deviations of $\Delta E(B - V)$ measured in the three WF chips are given in Table 4, separately for RC and UMS stars. The table reveals that the average extinction appears to not vary much in the field, although in chip WF 2 its value is marginally lower. The fact that RC stars have both lower and higher extinctions than the UMS objects suggests that they are not directly correlated with the absorbing material and that

Table 4. Statistics on the extinction towards RC and UMS stars across the observed field. For each of the three WF chips (see Figure 13), the table gives the number of stars (N) in the RC or UMS sample (Type) and some statistics on the extinction towards these objects, namely the minimum (Min), maximum (Max), average (Avg) and standard deviation (Stdev) of the measured $\Delta E(B - V)$.

Chip	Type	N	Min	Max	Avg	Stdev
WF 2	RC	46	0.04	0.69	0.21	0.13
WF 3	RC	32	0.04	0.77	0.26	0.17
WF 4	RC	27	0.02	0.53	0.23	0.12
WF 2	UMS	31	0.12	0.32	0.20	0.05
WF 3	UMS	112	0.11	0.41	0.25	0.07
WF 4	UMS	30	0.13	0.41	0.25	0.07

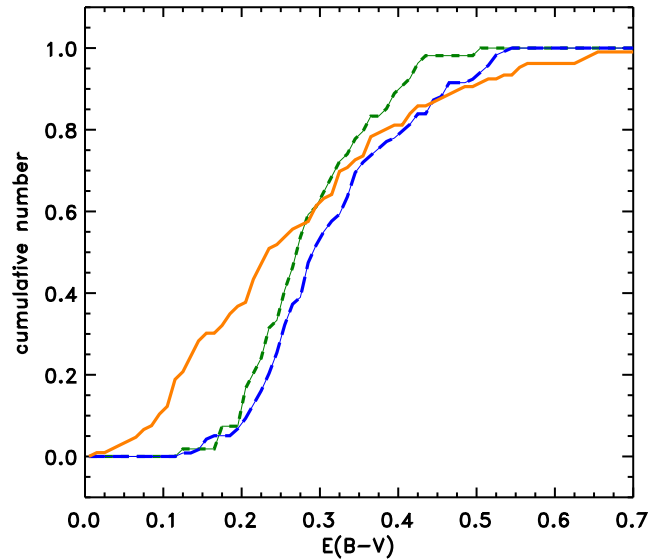


Figure 14. Cumulative distributions of the RC stars (solid line, orange in the online version), UMS stars in the small cluster (short-dashed line, green in the online version) and other UMS stars in the field (long-dashed line, blue in the online version). A Kolmogorov–Smirnov test shows that the probability that RC and UMS stars are drawn from the same underlying distribution is very small, $P = 7.2 \times 10^{-5}$.

they are distributed everywhere: within the cloud that envelopes the UMS stars and both in front and behind it. The absorbing material, on the other hand, is most likely associated with the UMS stars themselves or anyhow with the molecular cloud out of which they recently formed. It is, thus, not surprising that RC stars located behind the far edge of the molecular cloud show higher extinction.

To better quantify the difference in the reddening distribution of UMS and RC stars we show in Figure 14 the cumulative distributions of these objects, as a function of $E(B - V)$. A Kolmogorov–Smirnov test shows that the probability that RC and UMS stars come from the same distribution is very small, namely $P = 7.2 \times 10^{-5}$. As a sanity check we have also compared the distribution of the UMS stars in the cluster (short-dashed line) and over the rest of the field (long-dashed line), finding that they are indeed not significantly different ($P = 0.57$).

As mentioned above, Zaritsky (1999) reported that in the LMC stars with $T_{\text{eff}} > 12\,000$ K are typically affected by larger extinc-

tion values (several tenths of a magnitude more) than stars with $5\,500\text{ K} < T_{\text{eff}} < 6\,500\text{ K}$. Our results, therefore, appear at variance with Zaritsky's (1999) conclusions, since Figure 12 shows that the extinction towards RC stars can be considerably larger than that measured towards UMS objects. Note that we are confident about the nature of the RC objects, since we have only retained objects with $W_{\text{eq}}(H\alpha) < 3\text{ \AA}$ in order to carefully exclude PMS stars and other possible interlopers.

In fact, that the reddening is on average less severe for young stars than for the older objects was recently found by Sabbi et al. (2013) in the Tarantula Nebula, containing the 30 Dor region. As pointed out in that work, in his analysis Zaritsky (1999) only considered stars that were detected simultaneously in all four photometric bands U , B , V and I . This works as a bias against the more extinguished old stars, since they are the first ones to drop below the detection limit in the U band. Therefore, it is possible that in Zaritsky's (1999) study the average amount of reddening towards red giant branch stars might have been underestimated.

On the other hand, it is also possible that, with a field of view of $\sim 2'.7$ or $\sim 40\text{ pc}$ on a side, our observations do not sample a region wide enough to probe a statistically representative sample of UMS stars. For instance, the objects belonging to the small cluster have an even more limited spread of extinction than the other UMS objects in the field because they occupy a small volume along the line of sight and, more in general, this might be true for the entire young population in this field. Conversely, being older, stars like RC objects are more uniformly distributed. Since we are probing a particular region of the LMC, there is no certainty that our findings apply in general to this galaxy. We plan to extend this study to a much wider area, using existing high quality *HST* observations of the central regions of 30 Dor (De Marchi et al. 2011b) and of a large portion of the Tarantula Nebula (Sabbi et al. 2013). These observations will allow us to determine the reddening distribution towards both UMS and RC stars over a region of active star formation, covering almost 1% of the entire area of the LMC.

7 SUMMARY AND CONCLUSIONS

We have studied the properties of the interstellar extinction in a field of about $2'.7$ on a side located about $6'$ SW of 30 Dor in the LMC. The observations with the WFPC 2 on board the *HST* in the U , B , V , I and $H\alpha$ bands show the presence of patchy extinction in this field. In particular, the CMD reveals an elongated stellar sequence, running almost parallel to the MS, which is in reality made up of RC stars spread across the CMD because of the considerable and uneven levels of extinction across this region. This allows us to derive in a quantitative way both the extinction law R_λ and the values of the absolute extinction A_λ/A_V towards about 100 objects, thereby setting statistically significant constraints on the properties of the extinction in this area. The main results of this work can be summarised as follows.

(i) Using theoretical CMDs of the same type as those presented by Girardi & Salaris (2001) and Salaris & Girardi (2002), but computed for the specific WFPC2 bands of our observations, and assuming a single stellar population, we have studied the expected behaviour of the mean RC as a function of age (from 1.4 Gyr to 3.0 Gyr) and metallicity (from $1/20 Z_\odot$ to Z_\odot). We show that metallicity, age and reddening affect the position of RC stars in different ways in the CMDs defined by our bands.

(ii) Our analysis shows that the magnitude of the RC is not affected considerably by the age of the stars, except at very low

metallicity. In bands longwards of $\sim 4\,000\text{ \AA}$ an increase of metallicity would move the RC along directions similar to the reddening vector. However this effect is small because even a change of metallicity by a factor of two would mimic a quite modest amount of reddening. This limited sensitivity of the RC to age and metallicity makes it easier to estimate the amount of reddening when there is considerable interstellar extinction ($A_V > 1$), since in this case the magnitude and colour displacement of the RC in the CMD due to extinction dominate over all uncertainties on metallicity and age.

(iii) To identify bona-fide RC stars, we have compared our observations in all bands with the theoretical CMDs for the metallicity range applicable to the LMC ($0.004 < Z/Z_\odot < 0.008$), taking into account the known distance modulus and intervening MW reddening. This allows us to define the region of the CMDs where reddening can place RC stars, finding 170 objects inside it. With an iterative procedure, we have reduced this number to a total of 107 bona-fide RC stars simultaneously classified as such in all CMDs and with combined photometric uncertainty $\delta_4 < 0.23\text{ mag}$. We have conservatively removed from this sample two bona-fide PMS stars, with $H\alpha$ excess emission in the range $10\text{ \AA} < W_{\text{eq}}(H\alpha) < 30\text{ \AA}$, and additional ten objects with $3\text{ \AA} < W_{\text{eq}}(H\alpha) < 10\text{ \AA}$ that might also be PMS stars.

(iv) In each CMD, the best linear fit to the distribution of the bona-fide RC stars provides the absolute extinction and the ratio R between absolute and selective extinction in the specific bands of our observations. Through interpolation at the wavelengths of the Johnson B and V bands, we have derived the extinction curve in the form $R_\lambda \equiv A_\lambda/E(B-V)$, in the range $\sim 3\,000\text{--}8\,000\text{ \AA}$. Adopting the parametrization of Cardelli et al. (1989) and Fitzpatrick & Massa (1999), in this wavelength range our extinction law is consistent with a value of $R_V = 5.6$ with an uncertainty of 0.3.

(v) Compared with the values reported in the diffuse Galactic interstellar medium, where on average $R_V = 3.1$ (Cardelli et al. 1989), and with those towards 19 lines of sight in the LMC explored by Gordon et al. (2003), where on average $R_V = 3.4$, our larger R_V value indicates a considerably flatter extinction law, which in turn implies that in this region larger grains dominate. Since larger R_V values are usually found in denser regions, it is possible that the specific area that we have studied is simply denser than those sampled in the LMC so far. More in general, it could be the result of systematically different conditions of the environments in the LMC as compared to the MW.

(vi) Having derived the extinction law in this region, we have compared the extinction towards individual RC and UMS stars in order to study the relative distribution of stars and dust in this field. We find that UMS objects span a narrower range of $E(B-V)$ values than RC stars, at variance with the conclusion of Zaritsky (1999) that in the LMC stars with $T_{\text{eff}} < 12\,000\text{ K}$ are typically affected by larger extinction than stars with $5\,500\text{ K} < T_{\text{eff}} < 6\,500\text{ K}$. While it is plausible that in Zaritsky's (1999) study the average amount of reddening towards red giants might have been underestimated (see Sabbi et al. 2013), it is also possible that we are probing a peculiar region of the LMC.

In summary, in this work we have shown how to use multi-band *HST* photometry of a resolved stellar population to efficiently derive simultaneously the extinction law and the absolute value of the extinction towards a large number of RC stars in a typical LMC field. When the distance to the sources and their metallicity range are known, which is the case of any field in the MC, the average location of the RC in a CMD can be used to derive the absolute extinction towards its individual members by comparison with the-

oretical models. We have shown how multi-band photometry, and particularly the inclusion of the U band, can be used to lift the degeneracy introduced by uncertainties on the age and metallicity. The results are statistically significant because several dozen RC stars are present in the average MC field.

Furthermore, when the amount of the extinction is high and variable across the field, like in the region that we have studied, also the extinction law can be accurately derived, in absolute terms. In general, when there is measurable extinction, even without an appreciable spread, one can still determine the extinction law from the displacement between expected and actual RC locations, as recently done for instance by Nataf et al. (2013; see also Udalski 2003 and Sumi 2004, and references therein) using the OGLE observations of the Galactic bulge. However, the determination in this case is less reliable, because the lack of a clear reddening track makes the identification of spurious systematic effects much harder.

The advantage of our method is that the RC stars that we consider in our study are all at the same distance, to within 1 %, that they have very similar intrinsic physical properties in all bands, and that we can derive the absolute value of the extinction without having to extend the observations to infrared bands. So far our investigation using this method has covered a single field near 30 Dor, in which we find a much shallower extinction law than so far reported for the LMC, corresponding to $R_V = 5.6 \pm 0.3$. We plan to apply this method to existing *HST* observations of the 30 Dor cluster and of the Tarantula nebula at large, in order to investigate whether this extinction law is characteristic of other regions of intense star formation in the MC.

ACKNOWLEDGEMENTS

We are grateful to Vera Kozhurina–Platais for her assistance with the analysis of the data, and to Ian Howarth, the referee, for insightful comments that have helped us to improve the presentation of this work. NP acknowledges partial support by STScI–DDRF grant D0001.82435.

REFERENCES

- Bessell M., Castelli F., Plez B., 1998, *A&A*, 333, 231
 Bless R., Savage B., 1972, *ApJ*, 171, 293
 Bouchet P., Lequeux J., Maurice E., Prevot L., Prevot-Burnichon M., 1985, *A&A*, 149, 330
 Brunet J., et al., 1975, *A&AS*, 21, 109
 Cannon R., 1970, *MNRAS*, 150, 111
 Cardelli J., Clayton G., Mathis J., 1988, *ApJ*, 329, L33
 Cardelli J., Clayton G., Mathis J., 1989, *ApJ*, 345, 245
 Cardelli J., Sembach K., Mathis J., 1992, *AJ*, 104, 1916
 Cole A., 1998, *ApJ*, 500, L137
 De Marchi G., Nota A., Leitherer C., Ragazzoni R., Barbieri C., 1993, *ApJ*, 419, 658
 De Marchi G., Panagia N., Romaniello M., 2010, *ApJ*, 715, 1
 De Marchi G., et al., 2011a, *ApJ*, 740, 11
 De Marchi G., et al., 2011b, *ApJ*, 739, 27
 Dopita M., et al., 1997, *ApJ*, 474, 188
 Dolphin A., 2000, *PASP*, 112, 1397
 Fitzpatrick E., 1998, in *Ultraviolet Astrophysics Beyond the IUE Final Archive*, ed. W. Wamsteker, R. Gonzalez Riestra (Noordwijk: ESA), 461
 Fitzpatrick E., 1999, *PASP*, 111, 63
 Fitzpatrick E., Massa D., 1990, *ApJS*, 72, 163
 Fitzpatrick E., Massa D., 1999, *ApJ*, 525, 1011
 Fitzpatrick E., Massa D., 2007, *ApJ*, 663, 320
 Fitzpatrick E., Savage B., 1984, *ApJ*, 279, 578
 Geha M., et al., 1998, *AJ*, 115, 1045
 Gilmozzi R., Panagia N., 1991, *MemSAIt*, 62, 965
 Girardi L., Groenewegen M., Weiss A., Salaris M., 1998, *MNRAS*, 301, 149
 Girardi L., et al., 2008, *PASP*, 120, 583
 Girardi L., Salaris M., 2001, *MNRAS*, 323, 109
 Gonzaga S., Biretta J., 2010, *HST WFPC2 Data Handbook*, Version 5.0, (Baltimore: STScI)
 Gordon K., Clayton G., Misselt K., Landolt A., Wolff M., 2003, *ApJ*, 594, 279
 Harris J., Zaritsky D., Thompson I., 1997, *AJ*, 114, 1933
 Haschke R., Grebel E., Duffau S., 2011, *AJ*, 141, 158
 Hill V., Andrievsky S., Spite M., 1995, *A&A*, 293, 347
 Iben I., 1974, *ARA&A*, 12, 215
 Isserstedt J., 1975, *A&A*, 41, 175
 Johnson H., 1968, in *Nebulae and interstellar matter*, ed. B. Middlehurst, L. Aller (Chicago: Univ. Chicago Press), 167
 Johnson H., Borgman J. 1963, *Bull. Astron. Inst. Netherlands*, 17, 115
 Kim S.-H., Martin P., Hendry P., 1994, *ApJ*, 422, 164
 Laidler V., et al., 2005, *Synphot User's Guide*, (Baltimore: STScI)
 Lim P., Chiaberge M., Biretta J., di Nino D., 2009, *Instrument Science Report WFPC2 2009-07*, (Baltimore: STScI)
 Linsky J., 1980, *ARA&A*, 18, 439
 Marigo P., et al., 2008, *A&A*, 482, 883
 Martin E., 1998, *AJ*, 115, 351
 Massa D., Savage B., Fitzpatrick E., 1983, *ApJ*, 266, 662
 McMaster M., Biretta J., 2008, *WFPC2 Instrument Handbook*, Version 10.0 (Baltimore: STScI)
 Micol A., et al., 2000, in *Astronomical Data Analysis Software and Systems IX*, ed. N. Manset, C. Veillet, D. Crabtree (San Francisco: ASP), 223
 Nataf D., et al., 2013, *ApJ*, 769, 88
 Paczynski B., 1986, *ApJ*, 304, 1
 Paczynski B., Stanek K., 1998, *ApJ*, 494, L219
 Panagia N., et al., 1987, *A&A*, 177, L25
 Panagia N., 1998, *MemSAIt*, 69, 225
 Panagia N., 1999, in *New Views of the Magellanic Clouds*, ed. Y.-H. Chu, N. Suntzeff, J. Hesser, D. Bohlender (San Francisco: ASP), 549
 Panagia N., De Marchi G., 2005, *BAAS*, 37, 1368
 Panagia N., Gilmozzi R., Macchetto F., Adorf H.-M., Kirshner R., 1991, *ApJ*, 380, L23
 Romaniello M., Panagia N., Scuderi S., Kirshner R., 2002, *AJ*, 123, 915
 Romaniello M., Scuderi S., Panagia N., Salerno R., Blanco C., 2006, *A&A*, 446, 955
 Sabbi E., et al., 2013, *AJ*, 146, 53
 Salaris M., Girardi L., 2002, *MNRAS*, 337, 332
 Savage B., Mathis J., 1979, *ARA&A*, 17, 73
 Scuderi S., Panagia N., Gilmozzi R., Challis P., Kirshner R., 1996, *ApJ*, 465, 956
 Seaton M., 1979, *MNRAS*, 187, 73P
 Stanek K., Garnavich P., 1998, *ApJ*, 503, L131
 Sumi T., 2004, *MNRAS*, 349, 193
 Tatton B., et al., 2013, *A&A*, 554, A33
 Udalski A., 2003, *ApJ*, 590, 284
 van de Hulst H., 1949, *Rech. Astr. Obs. Utrecht*, 11, part 2
 van de Hulst H., 1957, *Light Scattering by Small Particles*, (New York: Wiley)
 Wadadekar Y., et al., 2006, *PASP*, 118, 450
 Weingartner J., Draine B., 2001, *ApJ*, 548, 296
 White R., Basri G., 2003, *ApJ*, 582, 1109
 Zaritsky D., 1999, *AJ*, 118, 2824